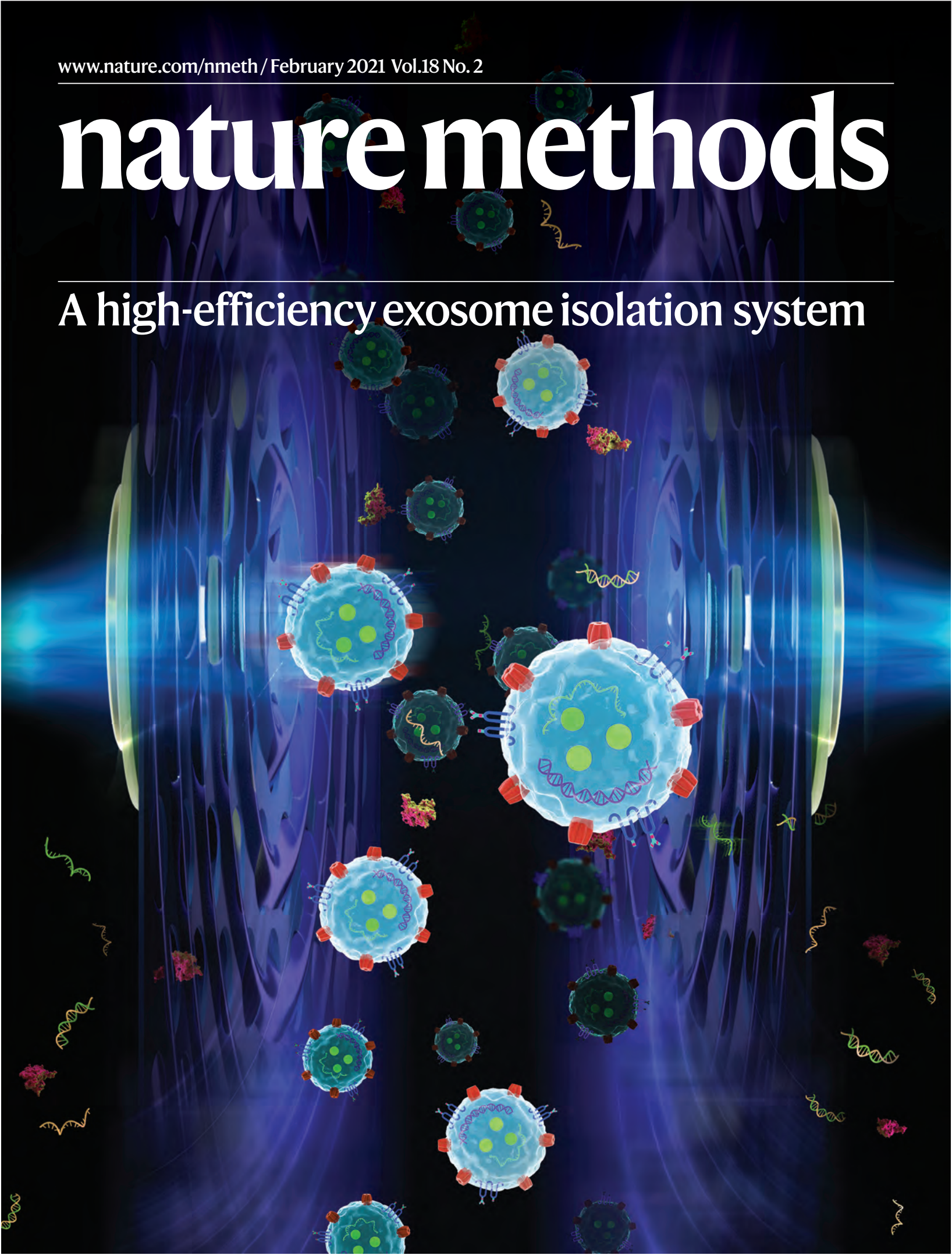


nature methods

A high-efficiency exosome isolation system





Exosome detection via the ultrafast-isolation system: EXODUS

Yuchao Chen^{1,2,9}, Qingfu Zhu^{1,9}, Liming Cheng³, Yong Wang², Meng Li⁴, Qinsi Yang², Liang Hu¹, Doudou Lou¹, Jiaoyuan Li³, Xianjun Dong⁵, Luke P. Lee^{6,7,8} and Fei Liu^{1,2}

Exosomes have shown great potential in disease diagnostics and therapeutics. However, current isolation approaches are burdensome and suffer from low speed, yield and purity, limiting basic research and clinical applications. Here, we describe an efficient exosome detection method via the ultrafast-isolation system (EXODUS) that allows automated label-free purification of exosomes from varied biofluids. We obtained the ultra-efficient purification of exosomes by negative pressure oscillation and double coupled harmonic oscillator-enabled membrane vibration. Our two coupled oscillators generate dual-frequency transverse waves on the membranes, enabling EXODUS to outperform other isolation techniques in speed, purity and yield. We demonstrated EXODUS by purifying exosomes from urine samples of 113 patients and validated the practical relevance in exosomal RNA profiling with the high-resolution capability and high-throughput analysis.

Exosomes are a particular category of extracellular vesicles (EVs) with a diameter of 30–150 nm secreted by most human cells; they serve as mediators of intercellular communication^{1,2}. Because of the biogenesis of exosomes, their content is a snapshot of a cell's life that reflects the intracellular composition of the cell origin. Recently, exosomes have emerged as a promising biomarker for tumor liquid biopsy^{3–5} and neurological diseases^{6,7}. Molecular cargo (for example, microRNAs, messenger RNAs and proteins) carried by body-cell-derived exosomes can reflect disease status and serve as essential biosignatures for early disease diagnosis^{8–11} and restorative therapy^{12,13}.

One of the main challenges of exosome isolation is eliminating nanoscale contaminants, including cell-free nucleic acids and lipoproteins, which interfere with exosomal biomarker interpretation¹. Ultracentrifugation¹⁴ is currently the main technique for exosome isolation. Still, it does not meet the standards required for clinical applications, mainly due to the low achievable exosome purity, yield, integrity and the lengthy processing time¹⁵. Other approaches^{15–21}, such as polyethylene glycol (PEG)-based precipitation, phosphatidylserine affinity capture, size-exclusion chromatography and membrane affinity, have emerged in recent years for particular applications, but with limited success¹⁵. Recently, the asymmetric flow field-flow fractionation method has been used for sorting subpopulations of EVs from culture media of cells and tumors with high resolution²², but its throughput is compromised by the tedious sample-preparation procedure. The increased requirement to the input EV concentration and the time-consuming process for single analysis also limit its wide applications. There is therefore motivation to develop innovative technologies to improve exosome purification in terms of efficiency, purity, yield, speed and robustness^{22,23}. Ultrafiltration-based techniques provide a potentially promising alternative, but they also have drawbacks. In tangential flow

filtration, a feed stream is made to flow parallel to a porous membrane to avoid clogging, as occurs in dead-end filtration²⁴. However, although tangential flow filtration has been used to concentrate exosomes from large volumes of conditioned cell culture media^{25–27}, it has rarely been considered for diagnostic purposes, mainly due to the cost of its disposable modules, the high shear stress involved²⁸, and the inflexibility in processing small sample volumes (for example, system dead volume).

This study presents a new ultrafiltration strategy to achieve clog-free and ultrafast purification of exosomes that overcomes the limitations of the other methods. We introduced double coupled harmonic oscillations into a dual-membrane filter configuration for the generation of transverse waves. The oscillation of nanoporous membranes and cartridge substantially inhibits fouling effects, which can otherwise lead to a decrease in the permeated flux, via acoustofluidic streaming, resulting in improved processing speed, yield and purity. Based on this mechanism, we established the rapid method of EXODUS (exosome detection via the ultrafast-isolation system), which consists of a low-cost disposable isolation device and a workstation. The automation of EXODUS is enabled by the workstation to allow simplified operation and superior robustness and reproducibility.

To confirm the efficacy of the EXODUS and its advantages over existing methods, we performed measurements on urine samples according to 'MISEV2018' guidelines³⁰ and EV-TRACK knowledgebase³¹. We then extended the EXODUS application to various biofluids, including plasma, saliva, culture medium and tears. We demonstrated the EXODUS's performance by processing 113 urine samples from patients with urinary cancer and control participants, followed by RNA sequencing (RNA-seq) for transcriptional profiling. Compared to existing methods applied to urine sample preparation, EXODUS has better speed, yield and purity; it can

¹Eye Hospital, School of Ophthalmology and Optometry, School of Biomedical Engineering, Wenzhou Medical University, Wenzhou, Zhejiang, China.

²Wenzhou Institute, University of Chinese Academy of Sciences, Wenzhou, Zhejiang, China. ³Department of Laboratory Medicine, Tongji Hospital, Tongji Medical College, Huazhong University of Science and Technology, Wuhan, China. ⁴College of Chemistry and Chemical Engineering, Xi'an University of Science and Technology, Xi'an, China. ⁵Department of Neurology, Brigham and Women's Hospital, Harvard Medical School, Boston, MA, USA. ⁶Renal Division and Division of Engineering in Medicine, Department of Medicine, Brigham and Women's Hospital, Harvard Medical School, Boston, MA, USA.

⁷Department of Bioengineering, Department of Electrical Engineering and Computer Science, University of California at Berkeley, Berkeley, CA, USA. ⁸Institute of Quantum Biophysics, Department of Biophysics, Sungkyunkwan University, Suwon, Korea. ⁹These authors contributed equally: Yuchao Chen, Qingfu Zhu. ✉e-mail: lpLee@bwh.harvard.edu; feiliu@wmu.edu.cn

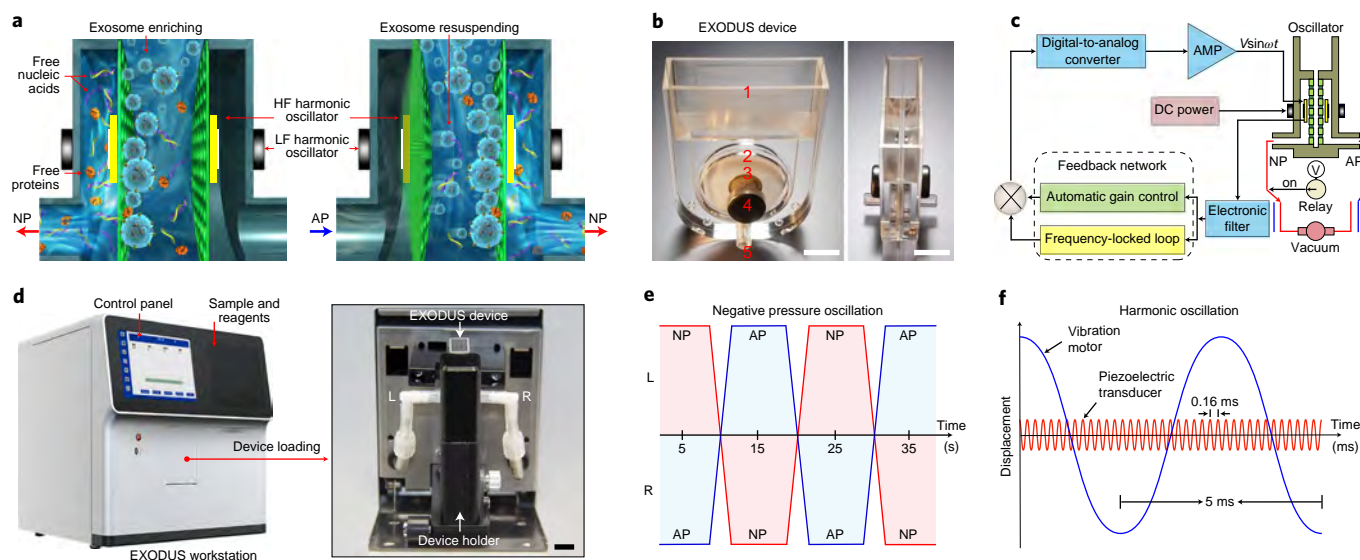


Fig. 1 | The hybrid macro- and nanomechanical oscillator-based exosome isolation system: EXODUS. **a**, The mechanism of NPO (AP, air pressure; NP, negative pressure). **b**, Photographs of the EXODUS device: 1, cartridge; 2, nanoporous membrane; 3, HF harmonic oscillator; 4, LF harmonic oscillator and 5, outlet (NP to AP switch). Scale bar, 1 cm. **c**, Schematic diagram of the control module for the resonator of EXODUS. **d**, A photograph of the EXODUS station, on which an EXODUS device is installed. Scale bar, 1 cm. **e**, The dynamic control of NP and AP applied to the two outlets (L and R) of the EXODUS device over time. **f**, The active regulation of coupled harmonic oscillators: low-frequency (via vibration motors) and HF (via piezoelectric transducers) on the EXODUS device.

process a wide range of specimen volumes for simultaneous exosome isolation, concentration and medium exchange, noninvasively and economically.

Results

Principle of device design and system operation. To achieve ultrafast exosome isolation, we designed EXODUS using a dual-filter sample reservoir with two outlets (L, left and R, right), each connected to a nanoporous anodic aluminum oxide (AAO) membrane. Periodic negative pressure oscillations (NPOs) are created on the AAO membrane by switching the direction of negative pressure (NP) and air pressure (AP) (Fig. 1a). The periodic NP switching from one side of the device to the other side serves two purposes. First, NP applied to the nanoporous membrane allows small particles (that is, proteins and nucleic acids) and fluids to pass through. Exosomes, which are larger, remain inside the central chamber (Fig. 1a, left). Second, as the NP is switched to AP, membrane vibrations induced by the immediate pressure increase favor the resuspension of the particles that were pressed onto the inner membrane surface by the fluid flow (Fig. 1a, right).

Outside the reservoir, a pair of piezoelectric transducers are integrated close to the membranes to generate high-frequency (HF) harmonic oscillations in nanoporous disk resonators (Fig. 1a,b and Extended Data Fig. 1a,b). Also, two vibration motors are attached concentrically on the cartridge for low-frequency (LF) harmonic oscillation of the entire device (Fig. 1a,b, Extended Data Fig. 1b,c and Supplementary Videos 1–3). With assistance from the two pairs of oscillators, the transverse waves and acoustofluidic streaming lift off the surface particles and resuspend them into the liquid, effectively limiting layer fouling and particle aggregations^{29,30}.

A schematic diagram of the control module, including NP and AP control and a feedback network consists of a frequency-locked loop and automatic gain control, was established to build the stable hybrid macro- and nanomechanical oscillators of the EXODUS device (Fig. 1c). The device, with nanoporous membranes and coupled harmonic resonators, is interfaced to an EXODUS station console (Fig. 1d and Extended Data Fig. 2), which integrates

fluidic and electronic components for automatic sample handling, the actuation of the device and process monitoring, allowing impurities to be excluded by nanopores²¹ (Supplementary Figs. 1 and 2). The NPO, HF and LF harmonic oscillations enabled by the console are shown in Fig. 1e,f.

Simulations and experimental results for EXODUS. Our simulations of fluid and pressure inside the EXODUS show a uniform flow rate distribution on both membranes with this configuration (Fig. 2a and Extended Data Fig. 3a,b). Our simulation of a pre-stressed vibrating membrane indicates that with acoustic waves at frequencies between 5,000 and 8,000 Hz, the circular membranes have a (0, 4) vibration mode^{31,32} (Extended Data Fig. 3c), which was verified experimentally by patterning microparticles on the membrane surface during oscillation (Fig. 2b). Because of this HF membrane oscillation, filter caking, which would otherwise reduce the filtration efficiency, is eliminated (Fig. 2c). The displacement of the membrane center over time can be described as

$$x(t) = A_0 \cos(\omega t + \varphi) \quad (1)$$

(ref. ³³), where the amplitude is expressed as

$$A_0 = \frac{F_0}{\sqrt{(k - m\omega^2)^2 + \gamma^2\omega^2}}, \quad (2)$$

in which F_0 , k , m , γ and ω are the amplitude of the external force, coefficient of stiffness, the mass of the vibrator, damping coefficient and vibration frequency, respectively (Supplementary Note 1). Equation (2) indicates that a higher liquid viscosity leads to a smaller vibration amplitude due to a more substantial damping effect (γ), which matches our simulation in Fig. 2d (blue curves).

Moreover, when the other parameters are determined, the amplitude of the oscillating membrane (A_0) is dependent on the vibration frequency (ω). The simulation shows that the amplitude peaks at 5,922 Hz would theoretically lead to the strongest membrane

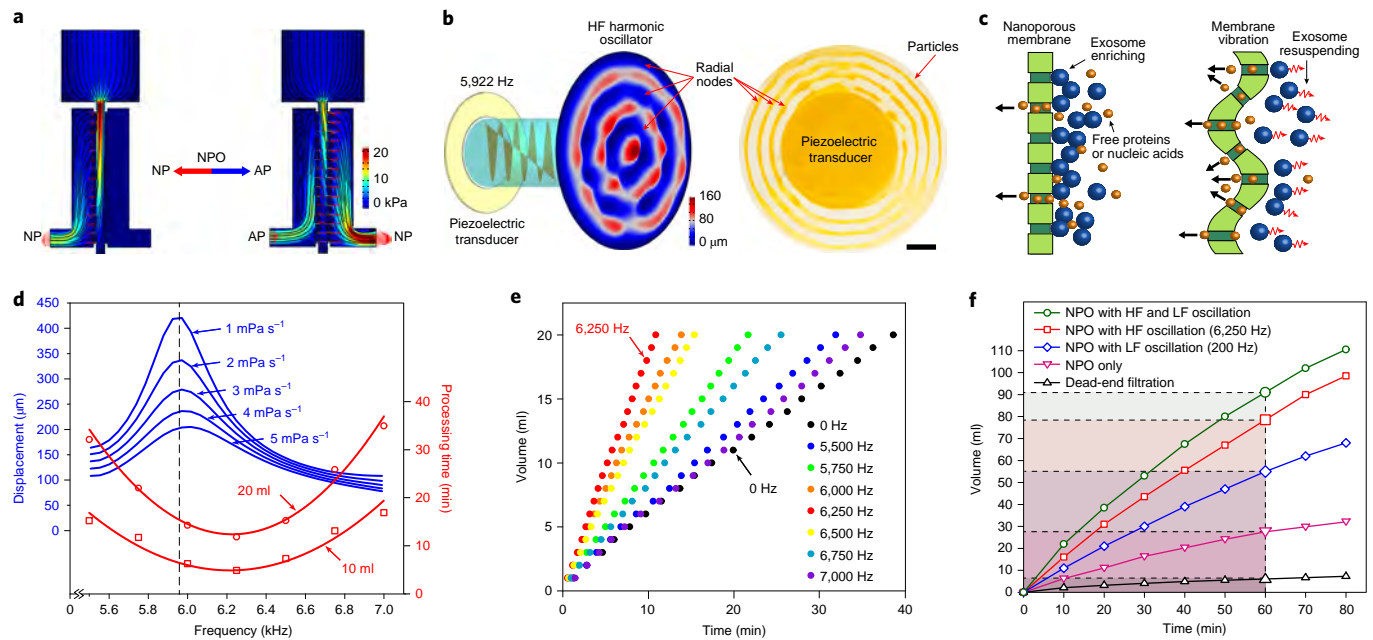


Fig. 2 | Mechanism and results of ultrafast purification via EXODUS with double coupled oscillators and the NPO. **a**, COMSOL simulation of the pressure distribution, fluidic streamline (black lines) and velocity (red arrows) inside the EXODUS device during NPO. **b**, Simulation and experimental verification of membrane oscillation at the resonant frequency of 5,922 Hz. Scale bar, 2.5 mm. **c**, Illustration showing that, with piezoelectric transducer-induced oscillation of the membrane, filter caking is eliminated during purification. **d**, Blue curves show simulation results of the oscillation response to the transducer signal for different fluid viscosities. Red data points and curves show experimental results with the excited resonating membranes, allowing us to minimize sample processing time at a frequency of 6,250 Hz. **e**, Comparison of the EXODUS device's separation efficiency at different oscillation frequencies of the membrane around the resonant peak (6,250 Hz). 0 Hz indicates that no AC waveform was applied. **f**, Comparison of the separation efficiency among EXODUS devices with and without integrating NPO, LF harmonic oscillation and HF harmonic oscillation.

vibration and therefore the best isolation performance (Fig. 2d). We processed 10 and 20 ml of urine samples by applying square AC waveforms ($10 V_{pp}$, where V_{pp} is the peak-to-peak voltage) ranging from 5,500 to 7,000 Hz. In our experimental studies, the fastest processing speed in both cases was observed at the frequency of 6,250 Hz (Fig. 2d, red curves), close to the theoretical value of 5,922 Hz. Time required to process 1 to 20 ml of urine samples with AC frequencies near 6,250 Hz is shown in Fig. 2e. The studies showed that membrane oscillations could generally reduce the processing time compared to that without acoustic actuation (0 Hz). Especially at the resonant frequency of 6,250 Hz in our design, about fourfold improvement in the processing speed was observed.

When subjected to the optimized NP of -30 kPa (Supplementary Fig. 3), the EXODUS device with NPO obtained an average urine processing speed of 28 ml h^{-1} (Fig. 2f, purple curve), which was around 4.6 times faster than dead-end filtration (6 ml h^{-1}) (Fig. 2f, black curve). In addition to the acoustic oscillation of nanoporous membrane, we integrated a pair of vibration motors onto the cartridge of EXODUS, offering harmonic oscillation to the entire device with a lower frequency (200 Hz) but much stronger displacement amplitude (Fig. 2f, blue curve). With the vibration motors, the transverse waves produced by the cartridge and membranes induced acoustic streaming in the liquids (Extended Data Fig. 1c and Supplementary Videos 1–3), substantially eliminated particle aggregation and surface binding, which also substantially improved the processing efficiency. Each oscillation mode contributes to improving the isolation efficiency, resulting in a total 15-fold increase of the average processing speed by combining all the oscillations (Fig. 2f, green curve).

EXODUS far outperforms the other exosome isolation technologies. To evaluate the performance of EXODUS relative to the

existing methods for exosome isolation, we compared EXODUS with current mainstream approaches: PEG precipitation, phosphatidylserine affinity, size-exclusion chromatography, membrane affinity and ultracentrifugation. The processing time, exosome purity and yield were considered the three primary performance metrics, plotted three-dimensionally for comparison (Fig. 3a). With the coupled triple resonators (that is, LF and HF oscillators and NPO), EXODUS reduced the processing time for 10 ml of urine samples from more than 80 min to less than 10 min (Fig. 2f), faster than the other techniques (Extended Data Fig. 4a). To compare the yield and purity, we performed western blots to determine the presence of exosomal proteins Alix, CD63, TSG101 and CD81. Uromodulin (UMOD)³⁴, a major protein contaminant in urine, was selected for purity verification. Equal-sample-volume analysis and equal-protein-amount analysis were used to characterize exosome yield (Fig. 3b and Supplementary Fig. 4a) and purity (Fig. 3c and Supplementary Fig. 4b), respectively. In both cases, a more prominent band intensity for exosomal proteins and a lower band intensity for UMOD indicate EXODUS's superior performance. For instance, phosphatidylserine affinity, which showed one of the better western blot results, gave 29.7 and 44.4% of the yield and relative purity of EXODUS, respectively; a membrane affinity technique with a comparable processing time (roughly 30 min) gave only 9.4 and 7.4% of the yield and relative purity of EXODUS, respectively. Silver staining further confirmed that EXODUS removed the most protein contaminants (Supplementary Fig. 5). By calculating the recovery rate, we found that roughly 99% of protein impurities had been removed after EXODUS purification of 15 ml of cell culture medium and roughly 90% of exosomes were recovered from exosome standards (Supplementary Fig. 6). All of the techniques showed a similar size distribution, ranging from 50 to 200 nm with a peak at approximately 100 nm, while the

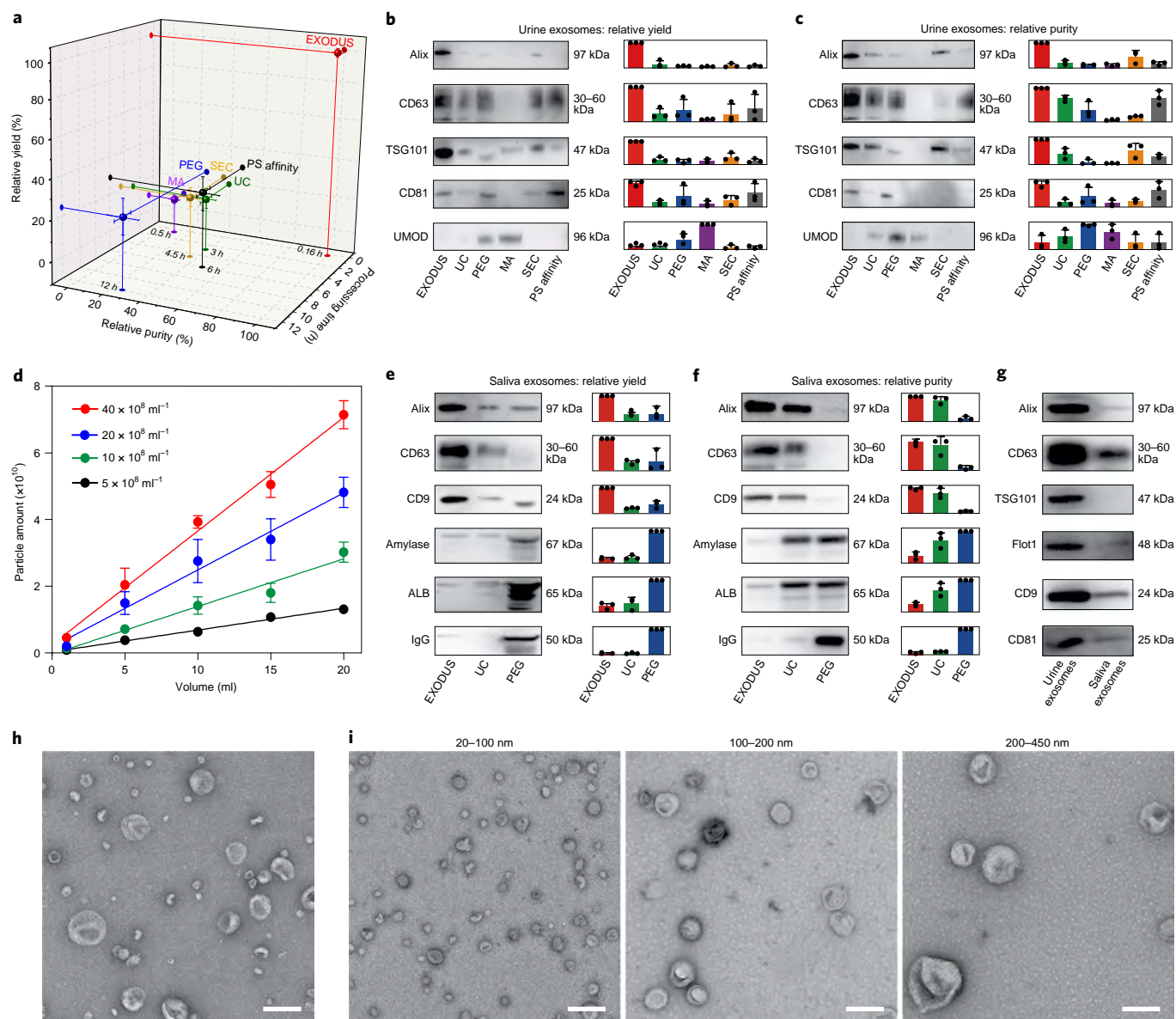


Fig. 3 | Characterization of EXODUS performance and comparison to other methods of exosome isolation. **a**, Three-dimensional comparison of yield, purity and processing time of EXODUS and other methods. Relative purity and relative yield were characterized by western blot results (left) and the relative band intensity (right) in **b** and **c** by comparing the total band intensities of exosomal proteins from the other techniques to that of EXODUS. UC, ultracentrifugation; PEG, PEG-based precipitation; SEC, size-exclusion chromatography; MA, membrane affinity; PS affinity, phosphatidylserine affinity capture ($n=3$ independent experiments from a urine pool of three donors). **b**, Equal sample volume (30 μ l of exosome sample equals 2 ml of urine). **c**, Equal-protein-amount (1,500 ng) western blot analysis of the expression of four common exosomal proteins (Alix, CD63, CD81 and TSG101) in samples prepared by EXODUS and other techniques. UMOD, the most abundant protein in the urine, was used as a contaminant reference for verifying exosome purity. Quantification of the normalized band intensities from three replications is shown in the right panel. **d**, Characterization of the particle yield as a function of the sample processing volume at different exosome concentrations ($n=3$ independent experiments from a urine pool of three donors). **e, f**, Western blot analysis (left) and the relative band intensity (right) of typical exosomal proteins (Alix, CD63, CD9) and protein contaminants (Amylase, ALB, IgG), from saliva exosomes prepared by EXODUS, ultracentrifugation and PEG ($n=3$ independent experiments from a saliva pool of three donors). Relative yield (**e**) and relative purity (**f**). **g**, Western blot analysis of urine exosomes and saliva exosomes with loading of equal protein amounts (1,500 ng). **h**, TEM image of exosomes isolated from a human urine sample using EXODUS. **i**, TEM images of EV subpopulations with three cut-off size ranges: 20–100, 100–200 and 200–450 nm (a urine pool of three donors). Scale bars, 200 nm. Data are presented as mean values \pm s.d.

EXODUS, PEG and membrane affinity methods collected more particles than others (Extended Data Fig. 4b,c). We also discovered that most UMOD was removed by EXODUS purification after the urine sample was stored at 4°C for 2 days, while a fresh urine or a sample stored at -80°C still showed UMOD contaminants (Supplementary Fig. 7).

To evaluate the stability and reproducibility of EXODUS, we processed four exosome samples at serially diluted concentrations in incremental volumes ranging from 1 to 20 ml (Fig. 3d). The particle numbers display a highly linear relationship to the input volume at all concentrations, demonstrating EXODUS's superior stability and the wide dynamic range of its workable sample

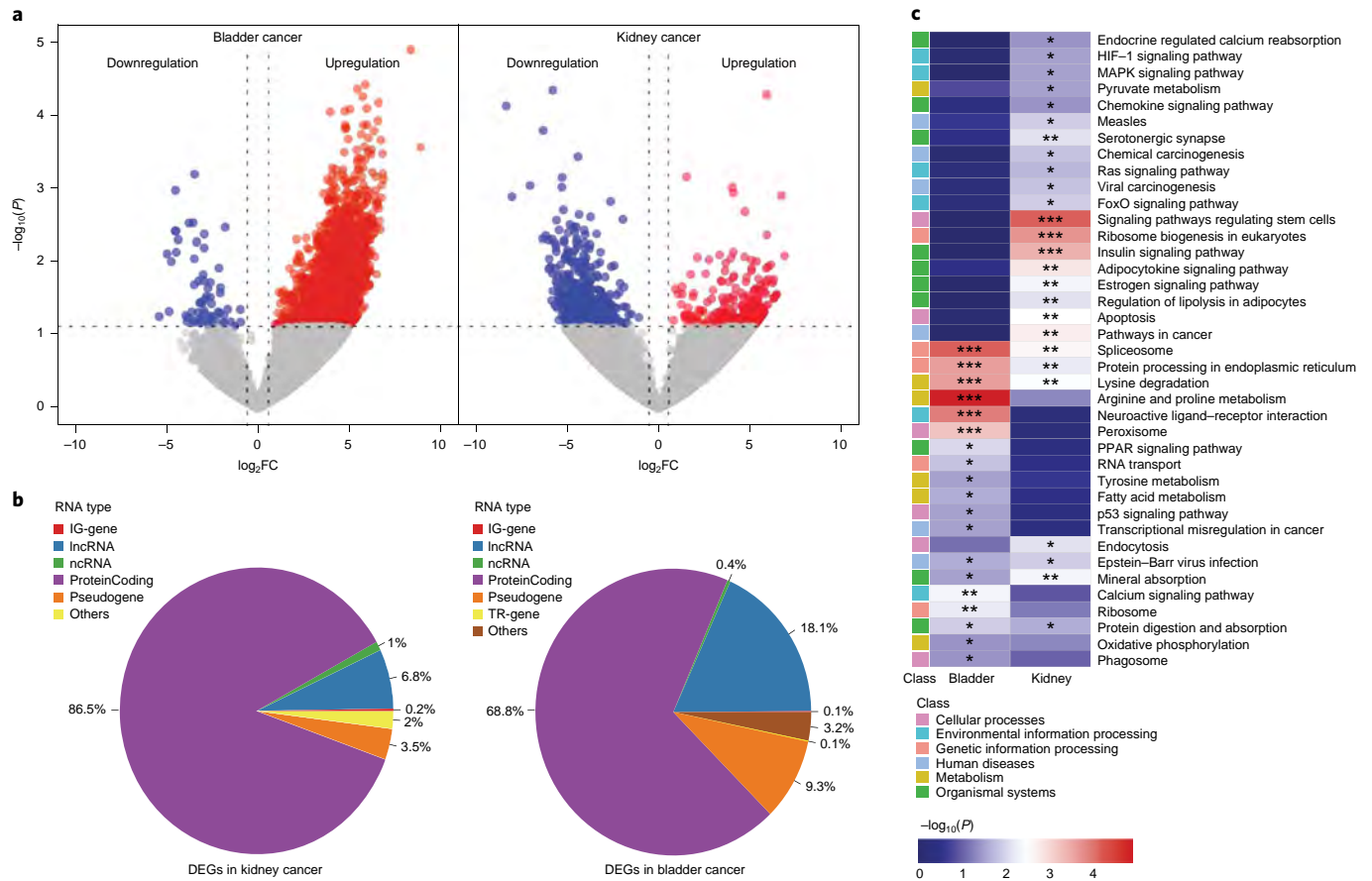


Fig. 4 | An example of EXODUS performance: profiling enriched pathways in bladder cancer and kidney cancer based on DEG analysis. a, Volcano plot showing DEGs in bladder cancer and kidney cancer. A false-discovery rate-corrected $P < 0.05$ and a fold change (FC) > 1.5 were used to define upregulation (red) and downregulation (blue) unless otherwise stated. Gray, not significant. **b**, Reads of the distribution of RNA biotypes from DEGs. lncRNA, long noncoding RNA; ncRNA, noncoding RNA. **c**, KEGG pathway analysis showing clear differences in enriched pathways between the kidney cancers and bladder cancer (* $P < 0.05$, ** $P < 0.01$ and *** $P < 0.001$ by unpaired Wilcoxon test, two-sided). The P values are provided in Supplementary Note 3. Each pathway term's statistical significance in the heatmap is colored red to blue to indicate high to low significance, respectively (kidney cancer, $n = 27$ biologically independent samples; kidney cancer control, $n = 31$ biologically independent samples; bladder cancer, $n = 35$ biologically independent samples and bladder cancer control, $n = 35$ biologically independent samples).

volume and concentration. Also, we repeated exosome isolation with 10 ml of urine aliquots 20 times and measured total protein amounts (Extended Data Fig. 4d). The coefficient of variation of the measurements was 9.9%, indicating good technical reproducibility of EXODUS.

The exosomes isolated by EXODUS were further inspected by transmission electron microscopy (TEM) (Fig. 3h). Most exosomes had good size integrity between 30 and 200 nm (Supplementary Fig. 8), consistent with previous reports³⁵. Unlike those from other isolation methods except for ultracentrifugation, EXODUS exosomes showed a round, cup-like structure¹⁴, validating the specificity of exosome isolation by EXODUS (Supplementary Fig. 9).

To investigate method versatility, we next extended EXODUS to isolate and purify exosomes from human saliva. Compared to those from ultracentrifugation and PEG methods, the exosomes purified by EXODUS showed more exosomal proteins (Alix, CD63, CD9) and lower amounts of protein contaminants such as amylase, albumin and IgG (Fig. 3e,f, and Supplementary Fig. 10). The TEM analysis shows a clean background and a typical cup-shaped morphology (Supplementary Fig. 11). We found that urinary exosomes carried much more protein than saliva exosomes (Fig. 3g and Supplementary Fig. 12). We also demonstrated

the isolation of exosomes from plasma, culture medium and tears, which had a wide variation in their volumes (0.02–110 ml) and concentrations of 10^8 – 10^{12} exosomes per ml, and also determined their typical size distributions (Extended Data Fig. 4e,f), indicating EXODUS is capable of processing various biofluids despite the different matrices.

To determine EV subtypes via EXODUS, we adjusted the membrane pore size and successfully identified three types of EV, in cut-off size ranges of 20–100, 100–200 and 200–450 nm, respectively (Fig. 3i and Extended Data Fig. 5).

Transcriptomic profiling of exosomes isolated from clinical urine samples. To verify high performance for practical application of EXODUS, we collected urine samples from patients with bladder cancer ($n = 35$) and kidney cancer ($n = 27$), as well as patients with noncancerous urinary diseases as control participants (35 for bladder cancer and 31 for kidney cancer) (Supplementary Table 1). We isolated exosomes from these clinical samples using our automated EXODUS. Nanoparticle tracking analysis (NTA) revealed that exosomes were in the 30–200 nm size range and the yields from patients with or without cancer were 10^9 – 10^{10} particles from 5 ml of urine (Supplementary Fig. 13).

We then profiled the exosomal transcriptome in 113 urine samples by EXODUS and ribo-depleted total RNA-seq (Methods) and investigated their RNA composition and enriched pathways. RNA-seq yielded an average read count of 30 million mapped reads per sample. Among the RNAs, we identified mRNAs (33.1%), long noncoding RNAs (21.9%) and pseudogenes (21.7%) as the most abundant biotypes based on retrieved annotations from the GENCODE database (Supplementary Fig. 14). We then calculated the differentially expressed genes (DEGs) in both cancers. By filtration with criteria of a P value <0.05 and a fold change >1.5 , we identified 1,922 DEGs for bladder cancer and 400 DEGs for kidney cancer, and found 28 shared DEGs between the two cancers. A volcano plot shows the DEGs for bladder cancer and kidney cancer (Fig. 4a). Most DEGs from exosomal RNAs are mRNAs, accounting for 86.5% of the DEGs in kidney cancer samples and 68.8% in bladder cancer samples. Long noncoding RNA was the second most abundant gene type, accounting for 6.8 and 18.1% of the DEGs in kidney cancer and bladder cancer, respectively (Fig. 4b). Overall, there were no significant differences in RNA type and read distribution between cancer and control samples (Supplementary Fig. 14b,c).

We then compared the enriched pathways in these two sets of cancer-associated exosomal RNAs. We found that Kyoto Encyclopedia of Genes and Genomes (KEGG) pathways involving energy and amino acid metabolism and protein synthesis and processing regulation were primarily enriched in the bladder cancer DEGs but not in kidney cancer DEGs (Fig. 4c). Simultaneously, the signaling pathway regulating stem cell pluripotency in cellular processes and ribosome biogenesis in eukaryotes pathways were found to be notably enriched only in kidney cancer. The metabolic pathway, as a cancer-related pathway³⁶, was found enriched in the DEGs for both kidney cancer and bladder cancer; the most enriched KEGG pathways and the number of involved DEGs are shown in Supplementary Fig. 15, and the gene ontology classification is summarized in Supplementary Fig. 16. We also investigated the enriched pathways from the WikiPathways community resource, in which we observed three significantly enriched pathways for kidney cancer and one for bladder cancer (Supplementary Fig. 17). The core genes involving the Notch signaling pathway, including *GATA3*, *GSK3B*, *MAML3* and *STAT3*, showed significant downregulation in kidney cancer, consistent with the previous findings³⁷. In the pathway of noncoding RNAs involved in Wnt signaling in hepatocellular carcinoma, related genes such as *EZH2* and *SFRP2* have also been reported to be upregulated in bladder cancer proliferation and metastasis^{38,39}.

Discussion

It has been emphasized that developing rapid, reliable and pure exosome isolation methods is urgent if we are to further advance the fundamental biological investigation and clinical translation of exosomes^{2,15,16}. Here we report EXODUS, a platform for ultrafast, high-performance exosome purification. Each oscillation mode introduced into EXODUS's membrane device, including NPO, LF and HF, contributes in a distinct manner to improving isolation efficiency in EXODUS. Therefore, we can set NPO or NPO combined with LF or with LF and HF harmonic oscillators on EXODUS devices to enrich and purify exosomes (or even viruses and bacteria) from different types and volumes of biofluids.

It has been reported that different isolation strategies tend to isolate a different subpopulation of exosomes due to their different principles⁴⁰. Our western blot analysis indicates that the exosomes isolated by EXODUS obtained the highest signal intensities from all of the selected exosomal proteins and the lowest signal intensity from the selected protein contaminant, showing the advantages of EXODUS in total exosome isolation and purification. Also, the EXODUS station's automatic operation allows a repeatable workflow and reproducible output for a wide range of sample types,

sample volumes and exosome concentrations. Therefore, via a new design and efficient system integration, EXODUS offers a robust method for convenient and rapid isolation of exosomes with unparalleled yield and purity, which markedly surpasses exosomes' current principal isolation techniques.

By applying EXODUS to the isolation of exosomes from urine samples from patients with kidney and bladder cancer for transcriptional profiling, we found pathways including those associated with metabolic reprogramming and protein processing in the endoplasmic reticulum for bladder cancer and with insulin signaling and adipocytokine signaling for kidney cancer, consistent with earlier studies^{41–43}, indicating the feasibility of EXODUS in clinical applications. Other identified enriched pathways, including spliceosome, peroxisome and ribosome biogenesis in eukaryotes, have not been reported as directly relating to urinary cancers and require for further evaluation.

We have identified features that would further improve the functionality of EXODUS in future studies. First, the current EXODUS platform is limited to single-channel isolation. Multi-sample processing via the implementation of an array of EXODUS devices with automatic reagent distribution and sample collection will benefit large-scale biological studies. Second, we have shown the potential of EXODUS in the study of exosome subtypes by applying three nanopore sizes (20, 100 and 200 nm). Further studies should allow specific isolation of exosome subpopulations with narrower intervals. Third, integration of EXODUS with downstream detection and analysis technologies (for example, quantitative PCR and immunoassay) will be favorable for high-speed, seamless enrichment and investigation of exosomes. In addition, further optimization of the reagents and isolation workflows for each individual sample type is necessary.

In conclusion, we present the EXODUS platform for ultrafast isolation of high-purity and high-yield exosomes from biofluids, which open avenues for exosome research in life sciences and speedy practical translations in medicine.

Online content

Any methods, additional references, Nature Research reporting summaries, source data, extended data, supplementary information, acknowledgements, peer review information; details of author contributions and competing interests; and statements of data and code availability are available at <https://doi.org/10.1038/s41592-020-01034-x>.

Received: 20 May 2020; Accepted: 30 November 2020;

Published online: 11 January 2021

References

1. Merchant, M. L., Rood, I. M., Deegens, J. K. J. & Klein, J. B. Isolation and characterization of urinary extracellular vesicles: implications for biomarker discovery. *Nat. Rev. Nephrol.* **13**, 731–749 (2017).
2. Wang, W., Luo, J. & Wang, S. Recent progress in isolation and detection of extracellular vesicles for cancer diagnostics. *Adv. Healthc. Mater.* **7**, 1800484 (2018).
3. Geurickx, E. & Hendrix, A. Targets, pitfalls and reference materials for liquid biopsy tests in cancer diagnostics. *Mol. Asp. Med.* **72**, 100828 (2020).
4. Mader, S. & Pantel, K. Liquid biopsy: current status and future perspectives. *Oncol. Res. Treat.* **40**, 404–408 (2017).
5. Lu, Y. T., Delijani, K., Mecum, A. & Goldkorn, A. Current status of liquid biopsies for the detection and management of prostate cancer. *Cancer Manag. Res.* **11**, 5271–5291 (2019).
6. Saeedi, S., Israel, S., Nagy, C. & Turecki, G. The emerging role of exosomes in mental disorders. *Transl. Psychiat.* **9**, 122 (2019).
7. Kanninen, K. M., Bister, N., Koistinaho, J. & Malm, T. Exosomes as new diagnostic tools in CNS diseases. *BBA – Mol. Basis Dis.* **1862**, 403–410 (2016).
8. Melo, S. A. et al. Glypican-1 identifies cancer exosomes and detects early pancreatic cancer. *Nature* **523**, 177–182 (2015).
9. Liang, K. et al. Nanoplasmonic quantification of tumor-derived extracellular vesicles in plasma microsamples for diagnosis and treatment monitoring. *Nat. Biomed. Eng.* **1**, 0021 (2017).

10. Li, Y. et al. Circular rna is enriched and stable in exosomes: a promising biomarker for cancer diagnosis. *Cell Res.* **25**, 981–984 (2015).
11. Zhu, L. et al. Exosomal tRNA-derived small RNA as a promising biomarker for cancer diagnosis. *Mol. Cancer* **18**, 74 (2019).
12. Zhang, Z. G., Buller, B. & Chopp, M. Exosomes—beyond stem cells for restorative therapy in stroke and neurological injury. *Nat. Rev. Neurol.* **15**, 193–203 (2019).
13. Qu, M. et al. Dopamine-loaded blood exosomes targeted to brain for better treatment of Parkinson's disease. *J. Control. Release* **287**, 156–166 (2018).
14. Momen-Heravi, F. Isolation of extracellular vesicles by ultracentrifugation. *Methods Mol. Biol.* **1660**, 25–32 (2017).
15. Li, X. et al. Challenges and opportunities in exosome research—perspectives from biology, engineering, and cancer therapy. *APL Bioeng.* **3**, 011503 (2019).
16. Guerreiro, E. M. et al. Efficient extracellular vesicle isolation by combining cell media modifications, ultrafiltration, and size-exclusion chromatography. *PLoS ONE* **13**, e0204276 (2018).
17. Woo, H. K. et al. Exodisc for rapid, size-selective, and efficient isolation and analysis of nanoscale extracellular vesicles from biological samples. *ACS Nano* **11**, 1360–1370 (2017).
18. Xu, R., Greening, D. W., Zhu, H. J., Takahashi, N. & Simpson, R. J. Extracellular vesicle isolation and characterization: toward clinical application. *J. Clin. Invest.* **126**, 1152–1162 (2016).
19. Heath, N. et al. Rapid isolation and enrichment of extracellular vesicle preparations using anion exchange chromatography. *Sci. Rep.* **8**, 5730 (2018).
20. Onódi, Z. et al. Isolation of high-purity extracellular vesicles by the combination of iodixanol density gradient ultracentrifugation and bind-elute chromatography from blood plasma. *Front. Physiol.* **9**, 1479 (2018).
21. Wu, M. et al. Isolation of exosomes from whole blood by integrating acoustics and microfluidics. *Proc. Natl Acad. Sci. USA* **114**, 10584–10589 (2017).
22. Li, P., Kaslan, M., Lee, S. H., Yao, J. & Gao, Z. Progress in exosome isolation techniques. *Theranostics* **7**, 789–804 (2017).
23. Konoshenko, M. Y., Lekchnov, E. A., Vlassov, A. V. & Laktionov, P. P. Isolation of extracellular vesicles: general methodologies and latest trends. *Biomed. Res. Int.* **2018**, 8545347 (2018).
24. Dalwadi, G., Benson, H. A. E. & Chen, Y. Comparison of diafiltration and tangential flow filtration for purification of nanoparticle suspensions. *Pharm. Res.* **22**, 2152–2162 (2005).
25. Busatto, S. et al. Tangential flow filtration for highly efficient concentration of extracellular vesicles from large volumes of fluid. *Cells* **7**, <https://doi.org/10.3390/cells7120273> (2018).
26. Colao, I. L., Corteling, R., Bracewell, D. & Wall, I. Manufacturing exosomes: a promising therapeutic platform. *Trends Mol. Med.* **24**, 242–256 (2018).
27. Andriolo, G. et al. Exosomes from human cardiac progenitor cells for therapeutic applications: development of a GMP-grade manufacturing method. *Front Physiol.* **9**, 1169 (2018).
28. Fernandez-Cerezo, L. et al. An ultra scale-down method to investigate monoclonal antibody processing during tangential flow filtration using ultrafiltration membranes. *Biotechnol. Bioeng.* **116**, 581–590 (2019).
29. Subramani, A., DeCarolis, J., Pearce, W. & Jacangelo, J. G. Vibratory shear enhanced process (VSEP) for treating brackish water reverse osmosis concentrate with high silica content. *Desalination* **291**, 15–22 (2012).
30. Petala, M. D. & Zouboulis, A. I. Vibratory shear enhanced processing membrane filtration applied for the removal of natural organic matter from surface waters. *J. Membr. Sci.* **269**, 1–14 (2006).
31. Macias, J. D., Ordóñez-Miranda, J. & Alvarado-Gil, J. J. Resonance frequencies and Young's modulus determination of magnetorheological elastomers using the photoacoustic technique. *J. Appl. Phys.* **112**, 124910 (2012).
32. Soares, R. M. & Gonçalves, P. B. Nonlinear vibrations and instabilities of a stretched hyperelastic annular membrane. *Int. J. Solids Struct.* **49**, 514–526 (2012).
33. Snowdon, J. C. Forced vibration of damped circular and annular membranes. *Tran. Socie. Rheol.* **15**, 685–707 (1971).
34. Wolf, M. T. F., Zhang, J. & Nie, M. Uromodulin in mineral metabolism. *Curr. Opin. Nephrol. Hypertens.* **28**, 481–489 (2019).
35. Lane, R. E., Korbie, D., Hill, M. M. & Trau, M. Extracellular vesicles as circulating cancer biomarkers: opportunities and challenges. *Clin. transl. med.* **7**, 14 (2018).
36. Boroughs, L. K. & DeBerardinis, R. J. Metabolic pathways promoting cancer cell survival and growth. *Nat. Cell Biol.* **17**, 351–359 (2015).
37. Sjölund, J. et al. Suppression of renal cell carcinoma growth by inhibition of notch signaling in vitro and in vivo. *J. Clin. Invest.* **118**, 217–228 (2008).
38. Knowles, M. A. & Hurst, C. D. Molecular biology of bladder cancer: new insights into pathogenesis and clinical diversity. *Nat. Rev. Cancer* **15**, 25–41 (2015).
39. Marsit, C. J. et al. Epigenetic inactivation of SFRP genes and tp53 alteration act jointly as markers of invasive bladder cancer. *Cancer Res.* **65**, 7081–7085 (2005).
40. Mateescu, B. et al. Obstacles and opportunities in the functional analysis of extracellular vesicle RNA—an ISEV position paper. *J. Extracell. Vesicles* **6**, 1286095 (2017).
41. Tracz, A. F., Szczylik, C., Porta, C. & Czarnecka, A. M. Insulin-like growth factor-1 signaling in renal cell carcinoma. *BMC Cancer* **16**, 453 (2016).
42. Horiguchi, A. et al. Leptin promotes invasiveness of murine renal cancer cells via extracellular signal-regulated kinases and rho dependent pathway. *J. Urol.* **176**, 1636–1641 (2006).
43. Hanahan, D. & Weinberg, Robert A. Hallmarks of cancer: the next generation. *Cell* **144**, 646–674 (2011).

Publisher's note Springer Nature remains neutral with regard to jurisdictional claims in published maps and institutional affiliations.

© The Author(s), under exclusive licence to Springer Nature America, Inc. 2021

Methods

Fabrication of EXODUS device for the isolation and purification. The cartridge of EXODUS was designed using SOLIDWORKS 2018 and molded into two identical parts with poly(methyl methacrylate) through computer numerical control milling. An AAO membrane was pasted on each part with a waterproof sealant (RTV4500, Silco Inc.). These two parts were then assembled via a buckle design and sealed with the same sealant. The devices contain two outlets connected to an open sample reservoir formed by two parallel, free-standing Whatman Anodisc filter membranes (diameters 13, 25 and 47 mm) and pore sizes of 20, 100 and 200 nm. The 47 mm type of AAO membrane was used for EXODUS method development, and 25 and 13 mm AAO membranes were used for processing saliva and clinical urine samples, respectively. Between each outlet and membrane, a piezoelectric transducer (a19011900ux0665, Uxcell) with a 9 mm diameter and resonant frequency of 3–7 kHz was attached to a three-dimensionally printed spacer that was close (roughly 0.5 mm) to the membrane. The electric connection of piezoelectric transducers to the function generator module was established via conductive silver epoxy (8331, MG Chemicals) through the EXODUS cartridge device. Two vibration motors (12,000 r.p.m., 1597-1244-ND, Digi-key) were attached on each side of the cartridge concentric with circular AAO membranes and powered by a 3 V d.c. Before processing urine samples, the device membrane was conditioned by flushing with 1 ml of 1× PBS twice.

Automatic station of EXODUS. The bespoke EXODUS station (Extended Data Fig. 2), which periodically generates alternating NP on the EXODUS device, is composed of a vacuum chamber and two solenoid valves. The function generator provides a square AC waveform with an amplitude of $10 V_{pp}$ at frequencies between 5,000 and 7,000 Hz. An autosampler is equipped to automatically deliver urine samples and washing buffers into the EXODUS device via the sample reservoir's opening. A 15- or 50-ml conical centrifugation tube containing a urine sample was placed inside the EXODUS station with a 4°C cooler to keep the sample fresh. The urine sample was continuously injected into the EXODUS device until the required sample amount had been processed. A liquid sensor on the sampling needle was used to detect the sample level and avoid overloading. The sampling needle was rinsed with deionized water after every injection to prevent contamination. All the parameters (NP intensity, pressure switching frequency and processing sample volume) are programmable via a control panel on the station.

Clinical samples. Participants were recruited according to a protocol approved by the Institutional Review Board of Tongji Hospital in the Tongji Medical College at Huazhong University of Science and Technology and gave their informed consent. Urine samples were collected from all participants: 35 patients with bladder cancer and 20 control patients with noncancerous bladder diseases; and 27 patients with kidney cancer and 16 control patients with noncancerous kidney diseases. The study group also included 15 individuals with other urinary diseases, such as urinary stone disease and benign prostatic hyperplasia, and other unknown urinary diseases as the shared participants for the two cancer groups. Patient information is summarized in Supplementary Table 1. Urine samples from healthy donors were collected for method comparison and optimization. Cancer diagnoses and stages were confirmed by histological examination and clinical imaging. Each urine sample was centrifuged at 2,000g for 10 min at 4°C. After that, the supernatant was filtered through a 0.22- μ m membrane filter (Millipore) and stored at –80°C until use. Before EXODUS isolation, dithiothreitol (Sigma-Aldrich) was added to the urine sample at a final concentration of 200 mM. The sample was then incubated at 37°C for 10 min to depolarize aggregated UMOD.

Exosome isolation with EXODUS. The detailed step-by-step EXODUS protocol for exosome isolation from different biofluids including urine, cell culture medium, human saliva, human plasma and tears is provided on Protocol Exchange⁴⁴. We used healthy donors' urine samples to optimize EXODUS with regard to sample storage conditions (fresh, 4°C, and –80°C), NP intensity and pressure switching time (Supplementary Figs. 3 and 7). Exosomes were purified from 10 ml of clinical urine samples with EXODUS at –30 kPa with a conversion time of 10 s. After exosome isolation, the collected exosomes were further washed via EXODUS with 1 ml of 1× PBS twice using the same optimized purification conditions. The purified exosome product was suspended in PBS at a final volume of 200 μ l and stored at –80°C until use. Immunoblotting was employed to evaluate exosomal proteins. The protein amounts were measured with a Qubit Protein Assay Kit (Invitrogen). A NanoSight NS300 (Malvern) was used to characterize the particle concentration and size distribution.

EXODUS isolation of exosomes from various biofluids. For exosome isolation from plasma sample, a 20 μ l plasma sample was diluted to 1 ml and then loaded on the EXODUS device for exosome isolation and collection. A pooled saliva sample was collected from healthy donors by Salivette following the manufacturer's instructions, and 1 ml of saliva sample was centrifuged at 2,000g for 10 min at 4°C before exosome isolation. The cell culture medium was collected from 293T cells (cultured without fetal bovine serum) at a confluency of 85%, and a 10 ml of the sample was centrifuged at 1,000g for 30 min at 4°C before exosome isolation. The pooled tear sample was collected from healthy donors by Schirmer's test following the manufacturer's instructions. The test paper (30 mm) was dissolved in 5 ml of

PBS and was centrifuged at 500g for 10 min and then 2,000g for 10 min at 4°C before exosome isolation. For the methods used to isolate exosomes using other technologies, refer to Supplementary Note 4.

Isolation of EV subpopulations. EV subtypes was isolated via EXODUS devices by adapting AAO membranes with different pore sizes. Three types of AAO membrane were selected, with pore sizes of 20, 100 and 200 nm. To separate EVs with a diameter of 20–100 nm, a 10 ml urine sample was prefiltered with a 100 nm syringe filter and then processed by an EXODUS device with a membrane pore size 20 nm. To obtain vesicles with a 100–200 nm diameter, a 10 ml urine sample was pretreated with a 220 nm syringe filter, then subjected to an EXODUS device with a membrane size of 100 nm. For the subtype 200–450 nm in diameter, a 450 nm syringe filter was used to treat 10 ml of urine, which was then subjected to an EXODUS device with a membrane size of 200 nm. Then 1× PBS buffer was used for washing and purification.

Determination of recovery rate. The EXODUS method's recovery rate was determined by isolating exosome standards via EXODUS, which was prepared by spiking exosomes with a known concentration into DMEM culture medium. In brief, 1 ml of exosome standards containing 3.44×10^{11} particles (measured by NTA) was loaded on the EXODUS device. After isolation, 1 ml of purified exosomes was collected from the EXODUS device and measured by NTA to determine the yield of isolation. The experiments were carried out with three replicates.

NTA. Exosome concentration and size distribution were determined using a NanoSight NS300 (Malvern) equipped with a 488 nm laser and a high-sensitivity sCMOS camera following the manufacturer's instructions. Each exosome sample was introduced to the instrument using a micropump with a syringe. Exosome samples purified via EXODUS were diluted 50 to 100-fold in 1× PBS to obtain roughly 50 particles in the field of view for optimal counting. Each sample was diluted in triplicate, and each diluted sample was analyzed three times with a capture time of 30 s. All NTA measurements were performed with identical system settings for consistency.

Western blot analysis. Western blotting was performed using 4–12% precast polyacrylamide slab mini-gels (tris-glycine, pH 8.3) in a Mini Trans-Blot module (Bio-Rad). Purified exosome protein was quantified using a Qubit Protein Assay Kit (Invitrogen). Protein lysates were resolved by SDS-PAGE and transferred onto polyvinylidene fluoride membranes (GE). Membranes were blocked for 1 h at room temperature, followed by primary antibody incubation overnight at 4°C. The following antibodies were used for western blot analysis: anti-CD63 (Abcam), anti-CD81 (Santa Cruz), anti-CD9 (Cell Signaling Technology), anti-Alix (Santa Cruz), anti-TSG101 (Novus), anti-flotillin (BD biosciences), anti-albumin (Santa Cruz), anti-IgG (Abcam), anti-UMOD (Abnova), anti-amyase (Santa Cruz) and anticalnexin (Abcam). All primary antibodies were used at a 1:1,000 dilution. The membranes were washed three times for 10 min (1× PBS and 0.5% Tween 20, pH 7.4) and then immersed in HRP-conjugated anti-mouse IgG or HRP-conjugated anti-rabbit IgG as the secondary antibody (1:3,000) for 60 min at room temperature. Imaging was performed using enhanced chemiluminescence for immunodetection (Peiqing Science & Technology). The original scans of blots are provided in Supplementary Data.

TEM analysis. Exosomes were fixed with 4% PFA and then transferred onto carbon grids. A 50- μ l drop of 1% glutaraldehyde was then transferred to each grid and incubated for 5 min. Afterward, the grids were washed with 100 μ l of distilled water. The adsorbed vesicles were stained with uranyl acetate (2%) for 30 s and then washed carefully with 1× PBS. After air drying, the samples were imaged with a transmission electron microscope (Talos F200S, Thermo).

RNA-seq analysis. Ribosomal RNA-depleted total exosome RNA was extracted from purified exosomes using a miRNeasy Mini Kit (Qiagen) according to the manufacturer's instructions. In brief, the purified exosomes were lysed by the addition of 750 μ l of TRIzol to the exosome sample, and the total RNA was extracted by 200 μ l of chloroform after sufficient mixing. After centrifugation at 12,000g, the sample's aqueous phase was loaded onto a RNeasy Mini column for RNA purification. RNA-seq libraries were generated using SMART technology (Clontech). Sequencing libraries were pooled and sequenced on the Illumina HiSeq platform. The sequencing length was 150 PE. Each time, roughly 80 samples were multiplexed in one lane, and 30 million reads per sample were acquired on average. The sequencing reads were aligned using HISAT2. Annotations of RNA types were retrieved from the GENCODE database⁴⁵. Differential gene expression analysis of each training set was performed by the DESeq2_1.22.2R package with default parameters. KEGG pathway, WikiPathways pathway and gene ontology term enrichment analyses were performed with WebGestalt (<http://www.webgestalt.org/>) using over-representation analysis with Fisher's exact test. The parameters for the enrichment analysis were as follows: (1) a minimum number of identifications in the category of 5, (2) a maximum number of identifications in the category of 2,000, (3) the false-discovery rate method of Benjamini and Hochberg and (4) a significance level of 'top 10'. Practical terms and pathways were statistically significant when $P < 0.05$.

Statistical analyses. Prism 8 and Origin 9.1 software were used for graphical representation and statistical analyses. The error bars in the graphical data represent the means \pm standard deviations. Numbers of experimental replicates are given in the figure legends. Statistical significance was determined using an unpaired Wilcoxon test (two-sided). $P < 0.05$ indicated statistical significance.

Numerical simulations. A three-dimensional model of the EXODUS device was constructed via SOLIDWORKS 2018 and then imported into COMSOL Multiphysics v.5.3a for numerical simulations of fluid dynamics and membrane forced vibration. The fluid was assumed to be viscous and compressible, with constant dynamic viscosity. Therefore, the governing equations of fluid motion were the compressible Navier–Stokes equations and the continuity equation. The circular membranes' vibration was considered as forced harmonic vibration and modeled via the governing equations of Bessel functions (Supplementary Note 2)¹⁶.

Reporting Summary. Further information on research design is available in the Nature Research Reporting Summary linked to this article.

Data availability

The data that support the findings of this study are available from the corresponding author upon request. The raw sequencing data are available at Genome Sequence Archive for Human with Bioproject ID [PRJCA003921](https://www.genome.gov/PRJCA003921) and data accession number [HRA000457](https://www.genome.gov/HRA000457). Source data are provided with this paper.

Code availability

The codes applied in this work are available at Zenodo⁴⁷ and github website at <https://github.com/sterding/EXODUS>.

References

- Chen, Y., Zhu, Q., Lee, L. P., & Liu, F. A protocol for exosome detection via the ultrafast-isolation system (EXODUS). *Protocol Exchange* <https://doi.org/10.21203/rs.3.pex-1263/v1> (2020).
- Frankish, A. et al. Gencode reference annotation for the human and mouse genomes. *Nucleic Acids Res.* **47**, D766–D773 (2019).
- Guo, H. et al. A highly sensitive, self-powered triboelectric auditory sensor for social robotics and hearing aids. *Sci. Robot.* **3**, eaat2516 (2018).
- Chen, Y., Zhu, Q., Lee, L. P., & Liu, F. Exosome detection via the ultrafast-isolation system: EXODUS. *Zenodo*. <https://doi.org/10.5281/zenodo.4268892> (2020).

Acknowledgements

We thank Tongji Hospital in the Tongji Medical College at Huazhong University of Science and Technology for providing clinical samples in this study. The work was primarily supported by research fund provided by the Zhenan Technology City Research Fund, the Zhejiang Provincial and Ministry of Health Research Fund for Medical Sciences (grant no. WKJ-ZJ-1910), the Wenzhou Medical University (grant no. 89218012) and the Wenzhou Institute, University of Chinese Academy of Sciences (grant no. WIBEZD2017006-05).

Author contributions

L.P.L. and F.L. conceived the project and designed the experiments. L.H., L.C. and J.L. organized and collected clinical samples. Y.C. designed the EXODUS device and workstation. Y.C., Q.Z. and Y.W. performed EXODUS system optimization. Y.C., Q.Z., Y.W., M.L. and Q.Y. purified and characterized urinary exosomes. L.H., D.L. and Q.Y. contributed to scanning electron microscopy and TEM analysis of exosomes. Y.W., Q.Y., Q.Z. and M.L. performed isolation method comparison, western blot analysis and NTA for urinary exosomes. Q.Z., Y.W. and Q.Y. performed EV subtype analysis. M.L., Q.Z. and Q.Y. isolated and analyzed saliva samples. M.L., Q.Z. and Q.Y. compared methods for analyzing saliva exosomes. Y.C. and Q.Z. determined the recovery rate. Y.C., Q.Z., M.L., Y.W., L.C., L.H., D.L. and X.D. contributed to data analysis and interpretation. L.C. and J.L. analyzed data related to clinical samples. Y.C. and Q.Z. wrote the manuscript. L.P.L. and F.L. edited the manuscript. All experiments were conducted under the supervision of L.P.L. and F.L. All authors read and approved the final manuscript.

Competing interests

The authors declare no competing interests.

Additional information

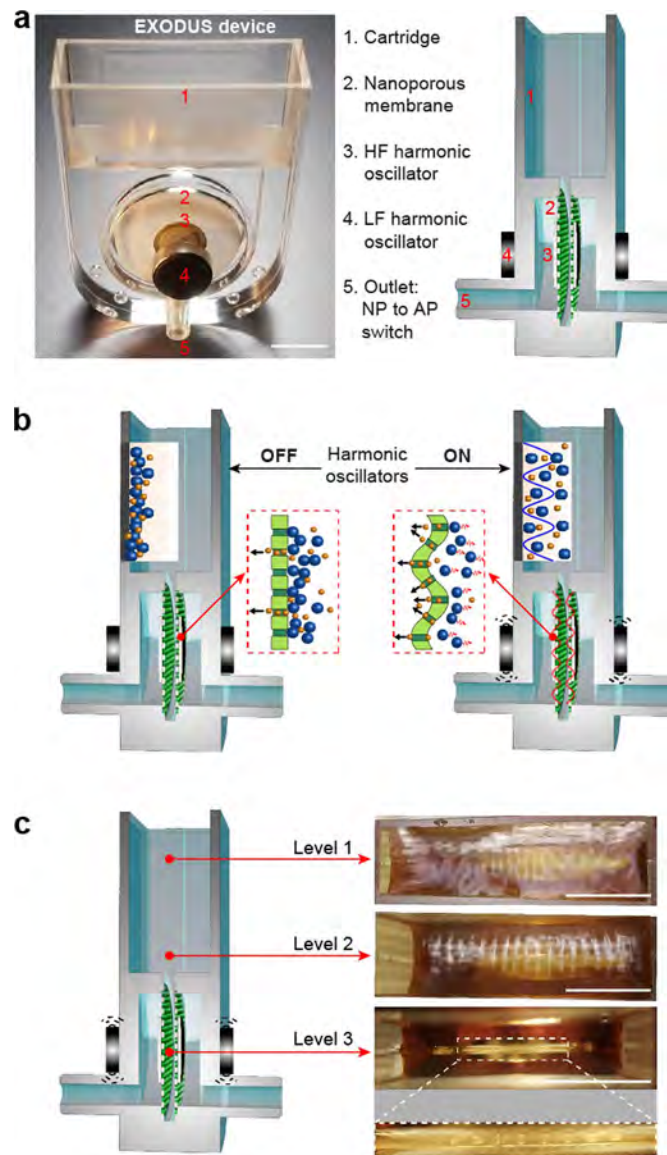
Extended data is available for this paper at <https://doi.org/10.1038/s41592-020-01034-x>.

Supplementary information is available for this paper at <https://doi.org/10.1038/s41592-020-01034-x>.

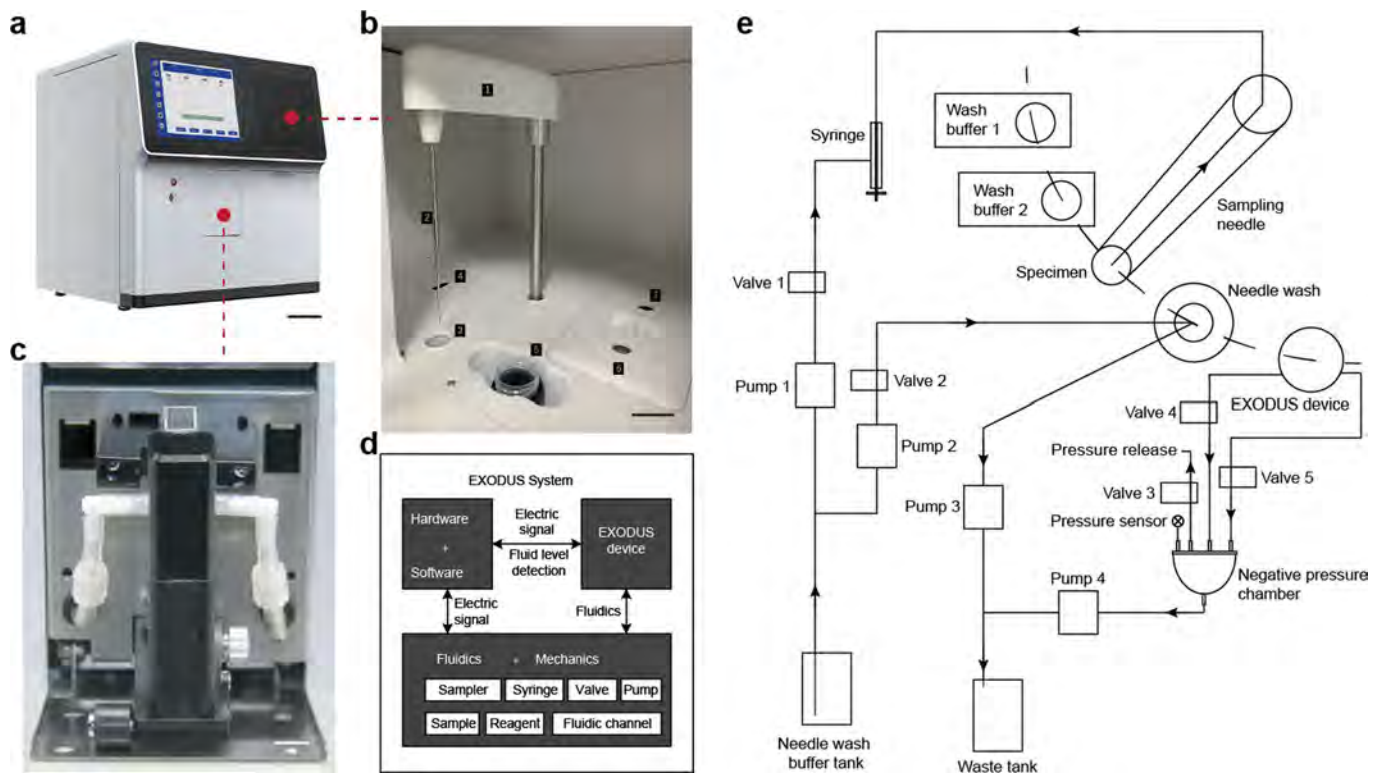
Peer review information Madhura Mukhopadhyay was the primary editor on this article and managed its editorial process and peer review in collaboration with the rest of the editorial team.

Correspondence and requests for materials should be addressed to L.P.L. or F.L.

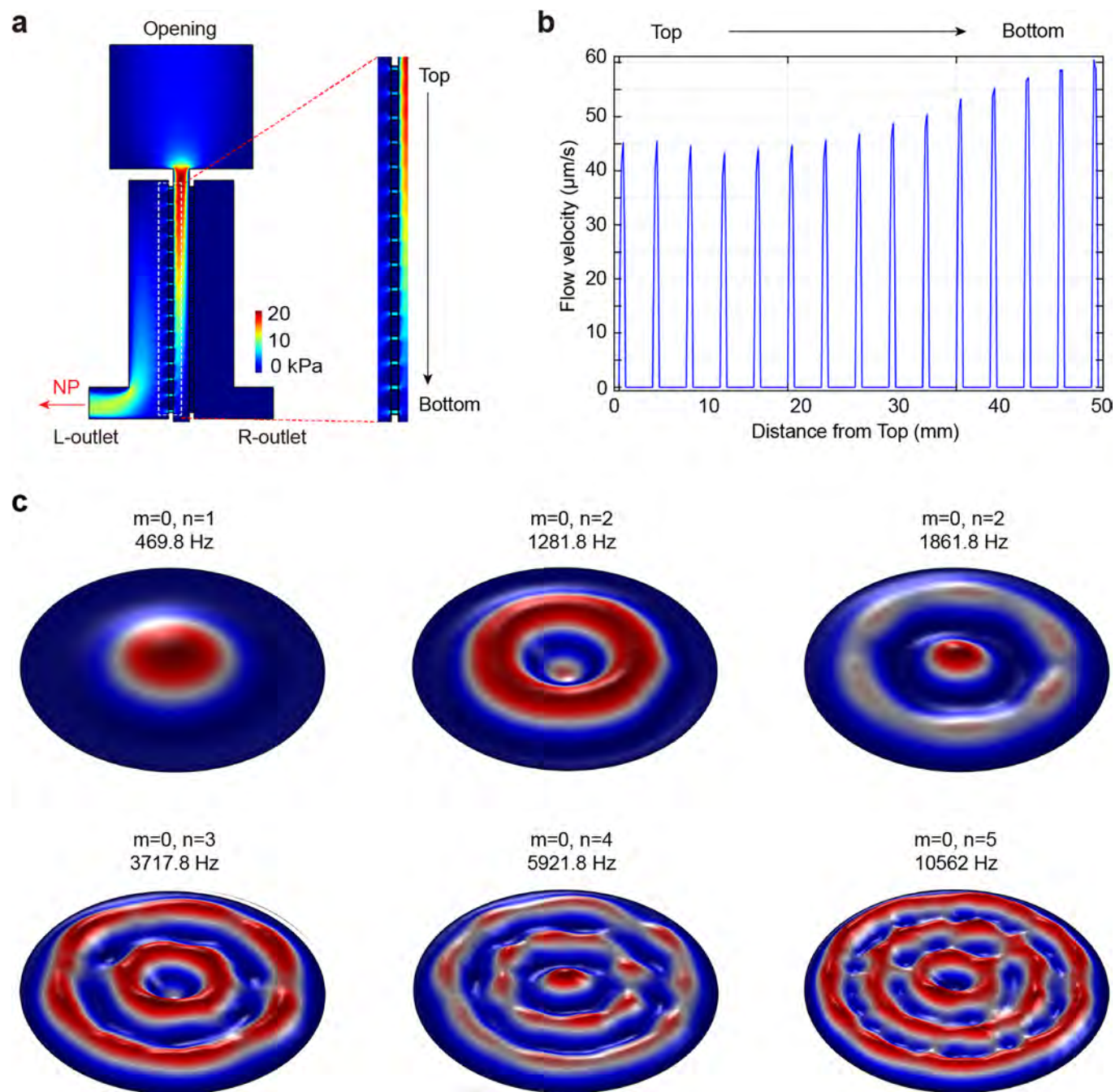
Reprints and permissions information is available at www.nature.com/reprints.



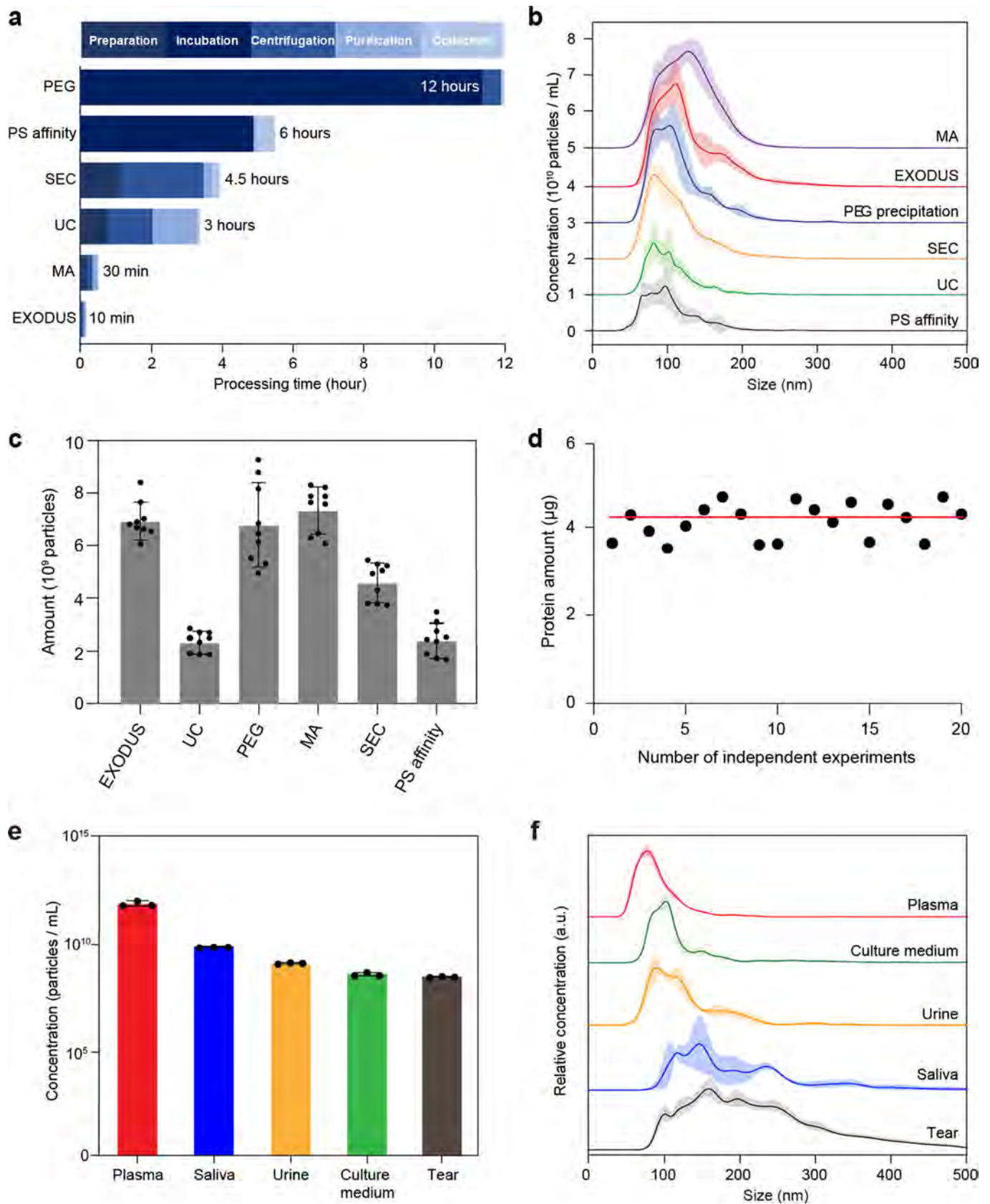
Extended Data Fig. 1 | Illustration of EXODUS device. a, A photo of the EXODUS device, with its cross-sectional illustration. Scale bar, 1 cm. **b**, Illustration of harmonic oscillations in the EXODUS device for minimizing fouling effect and bio-aggregates. **c**, The vibration motors generate acoustic streaming at different fluidic levels inside the EXODUS device. Scale bar, 1 cm.



Extended Data Fig. 2 | The system design of the EXODUS workstation. **a**, An image of the workstation. Scale bar, 10 cm. **b**, Internal view of the workstation, including (1) autosampler, (2) needle, (3) needle wash site, (4) EXODUS device window, (5) specimen tube, (6) wash buffer A, and (7) wash buffer B. Scale bar, 3 cm. **c**, The interface to EXODUS device via station: a device slot moves out from inside by pressing the button “Install Device” on the control panel to install EXODUS’s membrane device onto the workstation. **d**, The architecture of the EXODUS workstation. **e**, The illustration of the fluidic system in the EXODUS workstation.

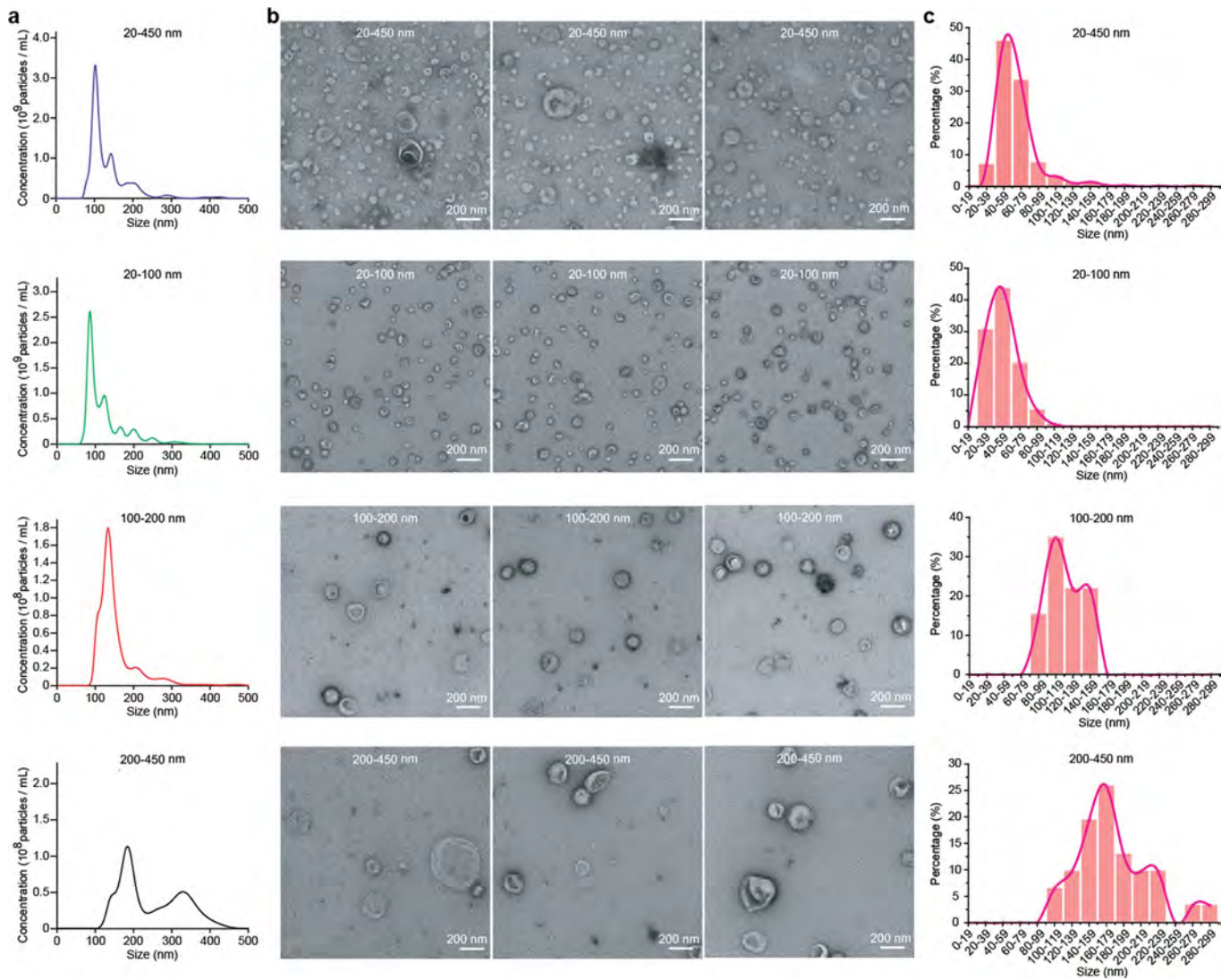


Extended Data Fig. 3 | Simulations of pressure, flow distribution, and vibration modes of the EXODUS device. **a**, COMSOL simulation showing the pressure distribution in a cross-section view of the EXODUS device when applying a -20 kPa negative pressure (NP) from the L-outlet. The sample is injected from the top opening into the sample reservoir. **b**, Distribution of flow velocity on the membrane from top to bottom. The flow velocity is between 45 and 60 $\mu\text{m/s}$, with a variation below 25%. **c**, Simulation of different vibration modes for a clamped circular nanoporous AAO membrane at their representative vibration frequencies: 469.8 Hz (5–700 Hz), 1281.8 Hz (700–1600 Hz), 1861.8 Hz (1600–3000 Hz), 3717.8 Hz (3000–5000 Hz), 5921.8 Hz (5000–8000 Hz), and 10562 Hz (8000–11500 Hz). The integer index m refers to the azimuthal node number. The index n refers to the n th non-trivial zero of the Bessel function. The high-frequency oscillation of the membrane at 6250 Hz by piezoelectric transducer has a (0,4) vibration mode, while the low high-frequency oscillation of the membrane at 200 Hz by vibration motor has a (0,1) vibration mode. The scale ranges from no displacement (dark blue) to maximum displacement (dark red).



Extended Data Fig. 4 | See next page for caption.

Extended Data Fig. 4 | Characterization of EXODUS. a, Comparison of the sample processing times of EXODUS and other methods showing their detailed procedures. For each method, the time cost was basically calculated according to its protocol. **b**, Size distributions and **c** amount of the particles obtained by EXODUS and other methods from 10 mL of urine sample aliquots. ($n \geq 5$ independent experiments). **d**, Isolation of exosomes from 10 mL of urine sample aliquots with 20 replications to study the reproducibility of EXODUS. Qubit™ Protein Assay Kits measured the total protein amounts of isolated samples, with an average protein amount of 4.3 μg and a CV of 9.9% over the 20 measurements. **e**, The concentrations and **f** size distributions of the particles isolated from different biofluids by EXODUS. ($n = 3$ independent experiments). The concentration of tear exosomes is presented as particles per centimeter tear collection paper. In **c** and **e**, data are presented as mean value \pm SD. NTA profiles in **b** and **f** are constructed by the average curve (solid line) and error band (shaded area).



Extended Data Fig. 5 | NTA and TEM analysis of EV subpopulations. **a**, NTA profiles of EV particles with various cut-off size ranges of 20–450, 20–100, 100–200, and 200–450 nm. **b**, The typical TEM images of vesicle subpopulations and the corresponding statistics of size distributions are summarized in **c**. (20–450 nm: $n = 565$ independent EVs, 20–100 nm: $n = 386$ independent EVs, 100–200 nm: $n = 46$ independent EVs, 200–450 nm: $n = 31$ independent EVs).